
EFFICIENT POWERTRAIN DESIGN — A MIXED-INTEGER GEOMETRIC PROGRAMMING APPROACH

A PREPRINT

Philipp Leise

Technische Universität Darmstadt
Chair of Fluid Systems
Department of Mechanical Engineering
philipp.leise@fst.tu-darmstadt.de

Peter F. Pelz

Technische Universität Darmstadt
Chair of Fluid Systems
Department of Mechanical Engineering
peter.pelz@fst.tu-darmstadt.de

February 24, 2021

ABSTRACT

The powertrain of battery electric vehicles can be optimized to maximize the travel distance for a given amount of stored energy in the traction battery. To achieve this, a combined control and design problem has to be solved which results in a non-convex Mixed-Integer Nonlinear Program. To solve this design task more efficiently, we present a new systematic optimization approach that leads to a convex Mixed-Integer Nonlinear Program. The solution process is based on a combination of Geometric Programming and a Benders decomposition. The benefits of this approach are a fast solution time, a global convergence, and the ability to derive local sensitivities in the optimal design point with no extra cost, as they are computed in the optimization procedure by solving a dual problem. The presented approach is suitable for the evaluation of a complete driving cycle, as this is commonly done in powertrain system design, or for usage in a stochastic approach, where multiple scenarios are sampled from a given probability density function. The latter is useful, to account for the uncertainty in the driving behavior to generate solutions that are optimal in an average sense for a high variety of vehicles and drive conditions. For the powertrain model we use a transmission model with up to two selectable transmission ratios and an electric motor model that is based on a scaled efficiency map representation. Furthermore, the shown model can also be used to model a continuously variable transmission to show beneficial energy savings based on this additional degree of freedom. The presented design approach is also applicable to a wide variety of design tasks for technical systems besides the shown use case.

1 Introduction

To improve the air quality, especially in cities, and to enable a more sustainable transportation, battery electric vehicles (BEVs) are a promising technology. With rapidly decreasing investment costs for the traction battery, as shown by [1], the profitability of these vehicles increases and therefore the number of new registrations. As a result the market share of electric vehicles increased over the last years, as shown by [2]. This increase of new registrations of BEV is also driven by environmental protection regulations in major markets, like for example China, [3]. The major drawback of BEVs in comparison to vehicles with an internal combustion engine, as stated by [4], is a shorter travel distance. The lower ratio of stored energy to weight within the vehicles and the higher recharging times of BEVs in comparison to fuel powered vehicles lead to requirements to improve the overall efficiency of the powertrain as much as possible.

The optimization program for the design task to derive optimized powertrain configurations must also consider the usage phase, cf. [5], to derive meaningful system designs. Therefore, a combined component design and control problem has to be solved. Furthermore, we explicitly consider a multi-speed transmission to improve the system efficiency even further. This problem results in a non-convex Mixed-Integer Nonlinear Program (MINLP) which is

hard to solve to global optimality. As a result, often primal heuristics like a genetic algorithm (GA) or particle-swarm optimization are used to derive a (local-optimal) optimized solution. For this approach see e.g. [6], [7] and [8].

To derive global-optimal solutions more rapidly, we present a new approach that combines *Geometric Programming* (GP) and a *Benders Decomposition* to solve the given design task. This results in a separation of the overall non-linear and non-convex optimization program in a main Mixed-Integer Linear Program and a convex Nonlinear Program (NLP) as a subproblem. These are then solved in an iterative solution process, where the convex subproblem leads in each iteration to additional constraints within the main problem. The main problem, on the other hand, leads to new binary assignments within the subproblem. This iterative solution of smaller optimization problems in combination with the convexified system properties results in an increased solution speed in comparison to the original non-convex MINLP.

In the following, we present a brief overview about geometric programming and convex powertrain design. Afterwards, we present the new geometric programming model for a powertrain design, the developed Benders approach and a heuristic to derive good solutions fast. Then, we show an outlook on the usage of mixed-integer geometric programming in powertrain design and close with a conclusion and summary.

2 Geometric Programming

The presented optimization model relies on the geometric programming approach, which was first developed by Duffin, Peterson, and Zener in 1967, cf. [9]. It is a modeling approach in which a log-transformation is used to convert a non-convex nonlinear program in a convex program. This transformation is possible, as shown in [10], if the objective and constraints either consist of monomials

$$m(x) = \alpha_0 x_1^{\alpha_{11}} x_2^{\alpha_{21}} \dots x_n^{\alpha_{n1}}, \quad (1)$$

or posynomials

$$p(x) = \sum_k \alpha_{0k} x_{1k}^{\alpha_{1k}} x_{2k}^{\alpha_{2k}} \dots x_{nk}^{\alpha_{nk}}. \quad (2)$$

In this example the n variables are given by x , while α represents specific parameters for each constraint and k the total number of terms of the sum. The underlying optimization program can be transformed in a convex program by using a log-transformation if it has a monomial as an objective and monomial or posynomial constraints of the following form, [10]:

$$\begin{aligned} \min_x \quad & m(x) \\ \text{s.t.} \quad & m(x) = 1 \\ & p(x) \leq 1 \\ & x > 0. \end{aligned} \quad (3)$$

The resulting log-transformed problem is convex. In general, convex programs can be solved very efficiently by state-of-the-art solvers. We refer to [10] as a general introduction on geometric programming and to [11] for an overview about convex optimization. The geometric programming approach is currently used in aircraft design, as for example shown by [12, 13].

Besides the geometric programming approach shown below, further research was done to derive convex optimization models for the powertrain component sizing and control. For instance [14] present a detailed modeling approach that relies on a convex optimization program. Additional approaches for convex modeling and optimization are given in [15], [16] and [17]. To the best of the author's knowledge, the powertrain design and control problem for battery electric vehicles with an explicit transmission ratio design has not yet been modeled as a (mixed-integer) geometric program. Hence, we present in the following section an easily extendable modeling approach, which is also compliant with the underlying physical principles.

3 Preprocessing

The powertrain of battery electric vehicles primarily consists of the battery, a power electronics, an electric motor and a transmission with one or more transmission ratios. For simplicity, we first present only the integration of a transmission with one variable single transmission ratio and an example electric motor. Further components are currently neglected, but can be added later, if necessary. In an early design stage in powertrain development commonly a backward dynamic longitudinal vehicle model is used to derive the torque and speed requirements at the wheel, [18]. In the

Table 1: Used vehicle parameters for dimensioning the powertrain.

PARAMETER	VALUE	UNIT	DESCRIPTION
M_0	1100	kg	vehicle mass
M_a	75	kg	additional component mass in powertrain
M_d	75	kg	mass of the considered driver
M_b	550	kg	mass of the used battery
g	9.81	m s^{-2}	specific gravitational constant
α	0	-	terrain slope angle
ρ	1.2041	kg m^{-3}	air density at 20 °C and sea level
c_w	0.3	-	drag coefficient
A	2.2	m^2	vehicle reference area
λ_r	0.01	-	rolling resistance coefficient
r	0.3	m	wheel radius
λ_i	1.0	-	inertia factor
η_g	0.98	-	efficiency of the gearbox
$\frac{\eta_g}{N^M}$	10000	min^{-1}	maximum speed of the selected motor

following we rely on a given driving load representation Λ :

$$\Lambda = \begin{bmatrix} \mathbf{v}^T \\ \mathbf{s}^T \\ \boldsymbol{\pi}^T \end{bmatrix}, \Lambda \in \mathbb{R}^{3 \times l}. \quad (4)$$

Here, \mathbf{v} represents the vector of velocity requirements and \mathbf{s} represents the slope requirements. This representation is equivalent to a given driving cycle representation, cf. [5], if the additional weights $\pi_t, t \in (1, \dots, l)$ are neglected. In the following we represent the set of used discrete time steps with \mathcal{T} . We can also interpret the given data representation as a finite event set approximation of a stochastic program with recourse. In this case an uncertain variable is given by the representation of a drive conditions. This interpretation enables us to evaluate multiple vehicle representations and drive conditions at once by using for instance specific weights π_t and not a driving cycle but a set of representative scenarios that approximate the underlying probability density function of the uncertain drive conditions. This set of scenarios is usually smaller than the complete cycle. This approach is useful in many situations, as most time steps in the driving cycle do not affect the final optimal solution. The usage of a comparable stochastic approach is for instance shown by [19] or [20].

We use the following longitudinal vehicle model for modeling the torque and speed requirements in the cycle [21, p. 83ff.]:

$$T_t = \left(\lambda_i m \dot{v}_t + mg (\sin(\alpha) + \lambda_r) + \frac{1}{2} \rho c_w A v_t^2 \right) r \quad \forall t \in \mathcal{T}. \quad (5)$$

We refer to Tab. 1 for the meaning and values of the used parameters. For the longitudinal vehicle model, we only use the speed v and acceleration \dot{v} in each time step in the given driving cycle as inputs. We derive acceleration values for each given discrete time step $t \in \mathcal{T}$ in the cycle based on a central difference scheme. For simplicity, we assume $s_t = 0 \forall t \in \mathcal{T}$. Nevertheless, this assumption can be easily dropped, as the modeling approach is independent of the slope values. It only differs in the preprocessing. As a reference cycle, we use in this section the *worldwide harmonized light vehicles test cycle* (WLTC), [22], as shown in Fig. 1. Furthermore, we only consider positive acceleration ($\dot{v} > 0 \text{ m s}^{-2}$) and speed ($v > 0 \text{ m s}^{-1}$) values in the following. We also present a further model extension to integrate recuperation in section 8.

As the power demand in the cycle depends on the total mass m of the vehicle, we can not estimate the power directly before optimization, if the used mass of relevant components are modeled as variables within the model. For a first approach, we use in this example a fixed value which is estimated as follows: $m = M_0 + M_d + M_a + M_b$. Here, M_0 is the basic vehicle mass, M_d the mass for the considered passengers, M_a the additional mass of powertrain components, and M_b the battery mass. Furthermore, we show a possible extension to a variable mass in section 8.

Within BEV, permanent magnet synchronous motors (PMSM) are commonly used, since they have a weight and efficiency benefit compared to other motor technologies. Therefore, the underlying electric motor model used in this contribution represents a PMSM. We use multiple monomials to represent specific power losses of the motor. For instance [23, 24] showed that PMSM partial losses, like the friction loss in bearings, or stray losses can be approximated by using monomials. As a reference for comparison, we use a scaled version of an efficiency map shown by [25] for a motor developed for the usage in electric vehicles. For simplicity, we currently do not model the power electronics and battery explicitly. Instead, we only use an aggregated efficiency map and assume that it represents the motor as well as the required power electronic components. We scale the derived efficiency map within the optimization according to the motor's maximum torque \bar{t}^M . This scaling is useful in the early design stage and

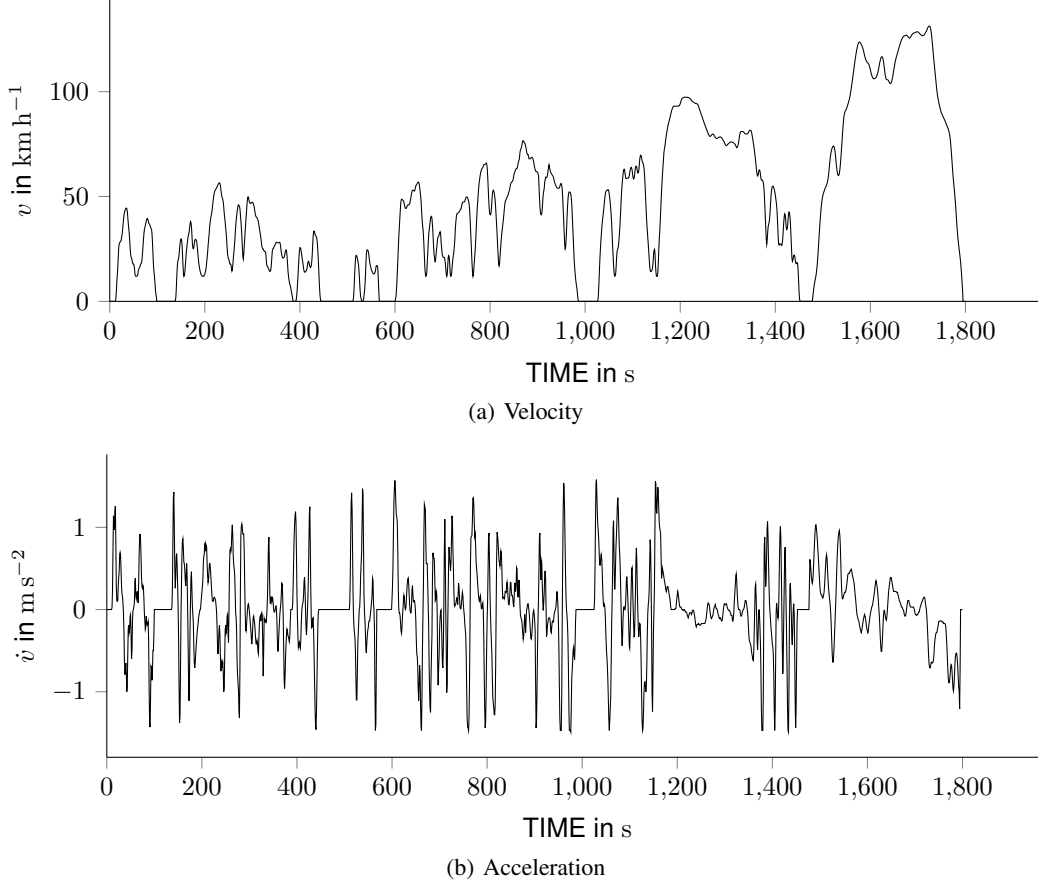


Figure 1: Input based on WLTC, [22]. (a) velocity requirements. (b) acceleration requirements derived by using a central difference scheme.

for instance also shown in [23]. It assumes that the efficiency map of a derived electric motor is comparable with the efficiency map of a reference motor of the same product series. The benefit of the shown approximation method is that it is compliant with the GP approach, as it is modeled with the help of multiple monomial and posynomial constraints. An example result of the used motor efficiency approximation method is shown in Fig. 2 for the 100 kW reference motor.

Next to the given driving cycle this optimization method allows to integrate easily further constraints, as for instance high speed requirements or starting constraints based on the gradeability on a slope. They can also be interpreted as further scenarios / time steps that must be met but have a zero probability π_t . This ensures that they are not accounted for in the objective but have to be fulfilled by the final solution.

4 Used Basic Model

The complete model is shown in description 4 in a condensed form. The used parameters, sets and variables are given in Tab. 2. The model reads as follows: As an objective, (6a), we consider an upper bound of the average approximation of the total power losses in all time steps \mathcal{T}^+ , which is given in constraint (6b). The transmission ratio i must lay between an upper bound \bar{I} and a given lower bound \underline{I} , (6c). Constraints (6d) and (6e) model the transmission with the variable transmission ratio i and the fixed gearbox efficiency η_g . We use the speed in min^{-1} of the given motor. If desired, it is also possible to use the angular speed $\omega^M = 2\pi n^M/60$ instead. As the motor can be scaled in the torque direction, we model the variable motor power with (6f) and the upper hyperbola limit of the feasible motor domain with constraint (6g). All torque values t^M and speed values n^M must lay in the feasible motor domain. Next to the previously modeled hyperbola, we also model the upper torque and speed limits in (6h) and (6i). As the efficiency map of the underlying PMSM should be scaled according to the maximum torque, we use a scaling parameter $k^{M,P}$ and introduce it in a monomial in constraint (6j). We use the motor power P_{ref} as a reference. Constraints (6k) – (6n)

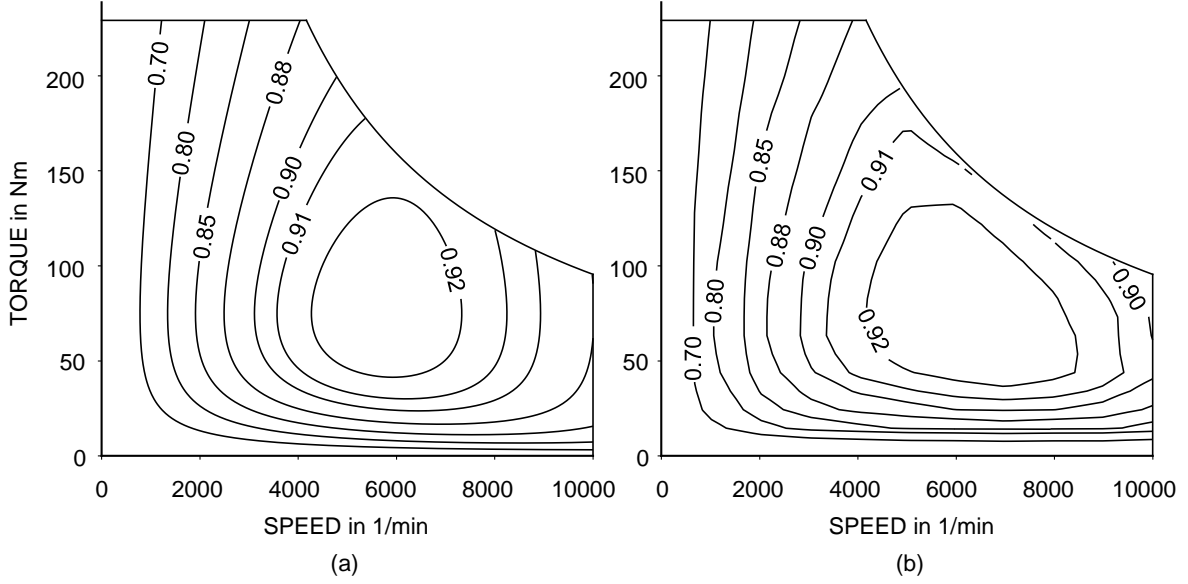


Figure 2: Comparison of used model and reference for the first quadrant of the efficiency map. The given values represent isolines with the same efficiency. (a) Output of the used GP-compatible efficiency map model for a motor with 100 kW. (b) Reference efficiency map of a given scaled motor with the same power, cf. [25].

represent specific power losses, based on the derived efficiency map model. We used a nonlinear least-square method to estimate the reference values and exponents. We use the scaling factor $k^{M,p}$ in each loss term to get an according scaling of all losses. The constant losses in constraint (6n) for instance can represent air gap losses and cooling power requirements, cf. [23]. These losses could be estimated with further scaling laws as well. Nevertheless, we omit these further details, as they don't affect the shown optimization approach and could be added later, if desired. The shaft power in each time step is given in (6o) and the total required power that must be supplied by the battery is given in a relaxed form in (6p). We additionally model an upper bound for $p^{M,in}$ in (6q). This upper bound is not active in the final result, but required for solving the GP. The complete model represents the physical properties of the given system. But especially the posynomial constraints (6b, 6p) have to be relaxed to allow the usage in the GP. Nevertheless, in the final solution they meet the equality condition to derive a system design that has the lowest power losses. Therefore, these constraint relaxations do not affect the found solution.

5 Exemplary Results for the Basic Model

We use the weights $\pi_t = 1/\sum_{k=1}^n 1 \forall t \in \mathcal{T}^+$ for each step based on the set \mathcal{T}^+ which was derived from the driving cycle. Here, we only consider positive speed and acceleration values, which results for the WLTC in 767 time steps. We additionally use two further restrictions, which must be fulfilled by the optimized powertrain. First a start torque at speed $n^M = 0.2 \text{ min}^{-1}$ that represents a gradeability on a slope of 66%. The speed value is set arbitrarily above zero to enable a GP solution. As the selected low speed value lays below the motor design speed, it does not affect the solution. Furthermore, we require a high-speed limit of 160 km h^{-1} with an acceleration of 0.3 m s^{-2} . These two constraints are modeled with two additional time steps, that must be fulfilled in the final motor domain, but are not used in the objective. In total, these 769 time steps result in approx. 6100 variables and approx. 20800 constraints for the complete program. The final transmission which is based on the WLTC, the required additional loads, and the given vehicle parameters in Tab. 1 has a transmission ratio of 7.06. The selected motor has a maximum power $\bar{p}^{M,out}$ of 185 kW which results in a maximum torque of $\bar{t}^M \approx 424 \text{ N m}$. These values are comparable with a solution derived by a genetic algorithm with a higher fidelity model that uses the original motor efficiency map next to recuperation.

Besides the specific transmission ratio i in the single-speed transmission, we can also consider a continuously variable transmission (CVT). In this case the transmission ratio is not modeled as a single variable but instead as a vectorized variable for all time steps. This additional degree of freedom results in a more efficient system design and can be seen as a physical lower bound for multi-speed transmission. We used an upper bound $\bar{I} = 18$ besides the lower bound $\underline{I} = 1.0$. In this domain, the optimized system design uses a motor with 73 kW and a maximum torque $\bar{t}^M \approx 167 \text{ N m}$.

Table 2: GP model notation

SET	DESCRIPTION		
\mathcal{T}	set of all considered time steps		
\mathcal{T}^+	set of all steps based on the given cycle		
PARAMETER	VALUE	UNIT	DESCRIPTION
η_g	0.98	–	transmission efficiency of gearbox
\bar{A}	0.4161	–	motor hyperbola constant
\bar{I}	1.0	–	minimum transmission ratio
\bar{I}	18.0	–	maximum transmission ratio
π	$1/\sum_{k=1}^l 1$	–	probability of occurrence for all $ \mathcal{T}^+ $ time steps in the given cycle
T^W	based on cycle	N m	wheel torque
N^W	based on cycle	min^{-1}	wheel rotational speed
\bar{N}^M	10000	min^{-1}	motor maximum rotational speed
P_{ref}	100	kW	power of reference motor
$P_{L,\text{ref},1}$	787.35	W	power reference loss 1
$P_{L,\text{ref},2}$	1566.67	W	power reference loss 2
$P_{L,\text{ref},3}$	9904.85	W	power reference loss 3
$P_{L,\text{ref},\text{const}}$	1059.34	W	power reference constant loss
\bar{P}^M_{in}	8000	kW	upper limit of required motor power
VARIABLE	DOMAIN	UNIT	DESCRIPTION
i	$[\bar{I}, \bar{I}]$	–	transmission ratio
t^M	$[0, \bar{t}^M]$	N m	motor torque
\bar{t}^M	\mathbb{R}^+	N m	motor maximum torque
n^M	$[0, \bar{N}^M]$	min^{-1}	motor speed
$p^{\text{M.in,avg}}$	\mathbb{R}^+	W	average used power in cycle
$p^{\text{M.in}}$	\mathbb{R}^+	W	motor power requirement drawn from battery
$\bar{p}^{\text{M.out}}$	\mathbb{R}^+	W	motor maximum design power
p^{M}	\mathbb{R}^+	W	motor design power
$k^{\text{M,p}}$	\mathbb{R}^+	–	motor power factor

The CVT result also reduces the objective value compared to the single-speed transmission by approx. 8%. This value depends on the given upper limit \bar{I} . Nevertheless, we can conclude that a CVT can improve the overall system performance. The usage of multiple transmission ratios in a BEV powertrain, which can be interpreted as a discrete approximation of the CVT, can result in potential energy savings, cf. [6].

We showed that the developed GP model is suitable for the early design stage of powertrain design. With the given model it is possible to compute optimized powertrain design solutions rapidly in comparison to a non-convex modeling or commonly used heuristics. We developed the model and preprocessing in Python. Therefore, we used Gpkit [26] for modeling and Mosek 9.2 as a solver. The computations were done on a Debian-based machine with an Intel i5-5200U and 12 GB RAM. On this hardware, we were able to compute the optimized system designs in less than three seconds each. This emphasizes the high potential for usage in rapid development in an early design stage.

6 Mixed-Integer Geometric Programming

Besides the already shown CVT and single-speed transmission, we can also derive solutions for multi-speed transmissions with this new design methodology. Therefore, we extend the shown CVT model in (4), by using two additional variables for the considered transmission ratios. Here, i_1 represents the first possible transmission ratio, while i_2 represents the second possible transmission ratio. Then, we can think of the final optimal solution having an optimal binary vectorized mapping $b_{t,g}$ for each time step $t \in \mathcal{T}$ and each transmission ratio $g \in \mathcal{G}$ with $\mathcal{G} = \{1, 2\}$. This binary decisions then indicate if either the first or second transmission ratio is chosen within the considered time step. This approach can also be extended to transmissions with more than two transmission ratios. For simplicity, we only restrict our description on the case of two transmission ratios.

The resulting MINLP has two stages. In the first stage, we assign the aforementioned continuous design variables. In the second stage, we then assign the aforementioned binary control variables for each time step to achieve a global optimal solution. As a result, we get a control strategy for the vehicle, based on the underlying dataset.

The second stage decision to assign transmission ratios to each time step is a combinatorial subproblem, that depends on the results of the first stage. This coupling between both stages in combination with the non-convex property within the original design space are the major challenges within the solution process of the underlying MINLP.

$$\begin{aligned}
\min \quad & p^{\text{M,in,avg}} & (6a) \\
\text{s.t.} \quad & \sum_{t \in \mathcal{T}^+} \pi_t p_t^{\text{M,in}} \leq p^{\text{M,in,avg}} & (6b) \\
& \underline{I} \leq i \leq \bar{I} & (6c) \\
& t_t^{\text{M}} i \eta_g = T_t^{\text{W}} & \forall t \in \mathcal{T} \quad (6d) \\
& n_t^{\text{M}} = i N_t^{\text{W}} & \forall t \in \mathcal{T} \quad (6e) \\
& \bar{p}^{\text{M,out}} = \bar{N}^{\text{M}} \frac{2\pi}{60} A \bar{t}^{\text{M}} & (6f) \\
& n_t^{\text{M}} \frac{2\pi}{60} t_t^{\text{M}} \leq \bar{p}^{\text{M,out}} & \forall t \in \mathcal{T} \quad (6g) \\
& n_t^{\text{M}} \leq \bar{N}^{\text{M}} & \forall t \in \mathcal{T} \quad (6h) \\
& t_t^{\text{M}} \leq \bar{t}^{\text{M}} & \forall t \in \mathcal{T} \quad (6i) \\
& k^{\text{M,p}} = \frac{\bar{p}^{\text{M,out}}}{P_{\text{ref}}} & (6j) \\
& p_t^{\text{M,L,1}} = k^{\text{M,p}} P_{\text{L,ref,1}} \left(\frac{t_t^{\text{M}}}{\bar{t}^{\text{M}}} \right) \left(\frac{n_t^{\text{M}}}{\bar{N}^{\text{M}} A} \right)^{3.93} & \forall t \in \mathcal{T} \quad (6k) \\
& p_t^{\text{M,L,2}} = k^{\text{M,p}} P_{\text{L,ref,2}} \left(\frac{t_t^{\text{M}}}{\bar{t}^{\text{M}}} \right) & \forall t \in \mathcal{T} \quad (6l) \\
& p_t^{\text{M,L,3}} = k^{\text{M,p}} P_{\text{L,ref,3}} \left(\frac{t_t^{\text{M}}}{\bar{t}^{\text{M}}} \right)^2 & \forall t \in \mathcal{T} \quad (6m) \\
& p_t^{\text{M,L,const}} = k^{\text{M,p}} P_{\text{L,ref,const}} & \forall t \in \mathcal{T} \quad (6n) \\
& p_t^{\text{M}} = t_t^{\text{M}} \frac{2\pi}{60} n_t^{\text{M}} & \forall t \in \mathcal{T} \quad (6o) \\
& p_t^{\text{M,in}} \geq p_t^{\text{M}} + p_t^{\text{M,L,1}} + p_t^{\text{M,L,2}} + p_t^{\text{M,L,3}} + p_t^{\text{M,L,const}} & \forall t \in \mathcal{T} \quad (6p) \\
& p_t^{\text{M,in}} \leq \bar{P}^{\text{M,in}} & \forall t \in \mathcal{T} \quad (6q)
\end{aligned}$$

Figure 3: GP model

In the following, we want to focus on the underlying combinatorial problem in the second stage and consider its complexity properties to derive approaches to improve the solution speed. As the assignment of a single transmission ratio to each time step (single-speed solution) is trivial, we will only consider transmissions that have at least 2 transmission ratios ($|\mathcal{G}| \geq 2$). We always assume, that $|\mathcal{G}| < |\mathcal{T}|$, as the assignment is otherwise (CVT solution) again trivial. All possibilities of an assignment of transmission ratios $g \in \mathcal{G}$ to time steps are described by the cartesian product, which results in

$$N_{g \rightarrow t} = |\mathcal{G}|^{|\mathcal{T}|}. \quad (7)$$

Nevertheless, this fast growing number of possible assignments, $N_{g \rightarrow t}$, can be reduced considerably, if we consider explicitly symmetry influences.

Symmetries in Integer Programs and Mixed-Integer Programs represent permutable variable assignments in the final solution, which lead to equivalent objective values and solutions, that are equivalent in terms of the final solutions properties. These symmetries lead to major difficulties for current state-of-the-art solvers that use a branch-and-cut approach as for example stated by [27]. These symmetries lead to a high number of equivalent enumerations within the solution process, which can reduce the solution speed considerably.

In our case, the presented MINLP has a high number of symmetric solutions, as the assignment of transmission ratios $g \in \mathcal{G}$ to each time step $t \in \mathcal{T}$ is equivalent, if we permute the assigned ratios in all time steps accordingly. The final solutions for each permuted assignment is equivalent, as each transmission ratio is optimized individually from each other. The final number of combinatoric solutions, after removing all symmetries, can be represented, in our case, by stirling numbers of the second kind, cf. [28, p. 243ff.] and [29, p. 66ff.]. These are used in combinatorics to derive the number of possibilities to assign a set of n distinguishable objects, in our case the time steps, into k nonempty

indistinguishable subsets, in our case the transmission ratios. Stirling numbers of second kind, $\left\{ \begin{smallmatrix} n \\ k \end{smallmatrix} \right\}$, are defined by:

$$S_{n,k} = \left\{ \begin{smallmatrix} n \\ k \end{smallmatrix} \right\} := \frac{1}{k!} \sum_{i=0}^k (-1)^i \binom{k}{i} (k-i)^n.$$

The final number of distinguishable combinatoric possibilities, without redundant symmetric assignments, is then considerably smaller, than proposed by Eq. (7). For the considered showcase of two-speed transmission the Stirling number then reduces to

$$S_{n,2} = \left\{ \begin{smallmatrix} n \\ 2 \end{smallmatrix} \right\} = 2^{n-1} - 1. \quad (8)$$

6.1 Brute Force Reference

One possibility for a small problem size is the usage of a brute force approach to solve all combinatoric possibilities. A fixed transmission ratio to time step assignment then reduces the MINLP to an NLP which can then be solved again by using the aforementioned approach.

To increase the solution speed of the brute force approach, we only compute assignments that are not symmetric, as stated before. This can be achieved with a lexicographic ordering of all binary assignments before optimization of each instance. We only consider the first half of all assignment vectors in the lexicographic ordering, as the second half corresponds to symmetric problem definitions. It is important to mention that this is only valid for two-speed transmissions. For three- or more-speed transmission the subset with all removed symmetric binary assignments has to be chosen differently.

Since even the Stirling number increases rapidly with the number of time steps, a brute force approach is only suitable for small problem instances with a low number of time steps. To recall, this small number of time steps can also be interpreted as specific scenarios, if the weights π_t within Eq. (4) are used within optimization. This reduced approach then is also often able to derive comparable results to the usage of a complete cycle.

Within this article, we only focus on the derived new design and solution methodology. We use the derived brute force solutions to evaluate the applicability of the Benders decomposition and heuristic solution approach more systematically.

6.2 Benders Decomposition

As a second solution approach, besides the brute force approach, we present the usage of a Benders decomposition, cf. [30] and [31]. It is suitable for the problem at hand, since it allows the exploitation of the specific problem structure given by the afore mentioned reference model. Within this approach, the MINLP is divided into two problems. One main problem in which all binary control decisions are selected and a subproblem in which all continuous design decisions are set. These problems are then solved iteratively and within each iteration specific information between both problems is shared. Here, the main problem is further constraint by so-called *optimality cuts*, which are derived from dual information within the subproblem. After reoptimization of the main problem a new binary assignment vector is transferred to the subproblem. After a new optimization this leads to new dual variable assignments in the intermediate solution and then to further new optimality cuts within the main problem.

6.3 Heuristic Solution Approach

As a third approach, we also present a heuristic, which uses an iterative assignment strategy. It uses the physical property that it is more efficient for a transmission ratio — time step assignment that low speed and high torque loads are assigned to the first transmission ratio, while high speed and low torque loads are assigned to the second transmission ratio. With this domain-specific knowledge, it is then possible to assign the time steps iteratively to each transmission ratio. The solution procedure starts with the CVT solution and then iteratively adds additional constraints for loads, starting with the highest torque and the highest speed loads. Since a fixation of the transmission ratios for specific loads leads usually to an infeasibility of the former CVT solution, we reoptimize the new model with its additional constraints. Then, the remaining unassigned loads in each time step are iteratively assigned based on the chosen transmission ratios and the difference to the chosen already fixed transmission ratios.

The result of the developed heuristic for the WLTC example, which we already used as a previous example, with 2 transmission ratios is shown in Fig. 4. It is able to derive an assignment for all loads within 21 iterations. The most assignments are done within the first iterations, while later iterations lead to the assignment of only a few remaining unset binary decisions.

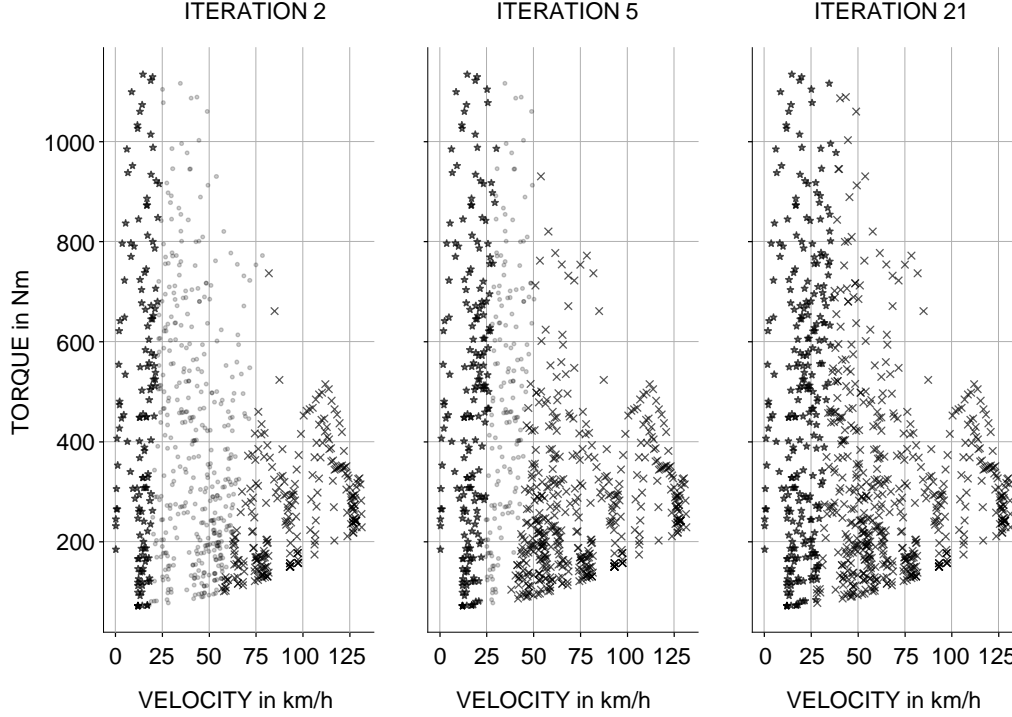


Figure 4: Result of the developed heuristic to derive near-global-optimal solutions for the WLTC. A star marks the usage of the first transmission ratio, while a cross shows the second transmission ratio. Unset binaries are marked with a circle. After 21 iterations all binary decision variables are set in this example.

7 Comparison of the Developed Solution Approaches

In the following, we present first results to show the applicability of the selected approaches. We compare the results and solution procedures of the Benders decomposition approach, the brute force approach, and the heuristic approach. Therefore, we used 6 – 12 scenarios in conjunction with the already shown model ((4)). To assure a more general understanding of the algorithms, we used 120 different instances. Here, we used the legislative driving cycles WLTC, Artemis Motorway, FTP75 and NYCC. Additionally, we use one cycle which is based on real driving behavior. It was derived by members of the institute of mechatronics systems at Technische Universität Darmstadt and we name this cycle “IMS Alltracks”. We refer to [32] for more details on the synthesis process. The scenarios were derived by using a k-means clustering approach based on the given datasets.

Within this section, we only focus on the algorithmic benefits and do not discuss any technical results that can be derived from the usage of the developed optimization approaches. This ensures a more concise overview on the algorithmic capabilities.

An overview of all instances is given in the Appendix in Table A1. The Benders decomposition approach is able to derive in all 120 test-cases the global-optimal solution, as resulting from the brute force approach. Additionally, a combination of the Benders decomposition and the heuristic is also able to derive the same global optimal solution. Nevertheless, the solution time can not be significantly improved by combining both, heuristic and Benders decomposition, on the given test-set. The Benders approach finds all solutions in a fraction of the required iterations of the brute force approach. Therefore, it is suitable for a more rapid solution procedure that can also derive global optimal solutions. The developed heuristic is also able to often derive the global optimal solution. Nevertheless, sometimes the resulting solution is only near-global optimal. But this near global optimality can also be effective for practical usage, where the solution time is a significant restriction.

Hence, we can conclude that the shown approaches are effective to derive global (in case of Benders decomposition) or at least near-global (in case of the heuristic) optimal solutions. We will evaluate the abilities on larger datasets and with an extended level of detail of the underlying model later. Therefore, we present further model extensions that can be used within the NLP (GP) and MINLP (MIGP) approach.

8 Model Extensions

With the help of the shown GP model we were able to transform the non-convex original problem to a convex program, without the need of further polynomial or piecewise-affine model approximations of components or the preliminary selection of transmission ratios. The underlying motor representation is based on physical properties of the modeled PMSM. The shown model (4) can be extended in multiple ways. For a more detailed mass estimation besides the shown fixed mass, we can model the total mass m , based on variable partial masses of different components. For instance, we can model the motor mass m^M with a specific mass ρ^M and the maximum motor power $\bar{p}^{M,\text{out}}$, as shown in constraint (9a). This results in a new variable mass m which can be estimated with fixed reference masses for the basic vehicle M_0 , for additional powertrain components M_a , for the passengers M_d , and for the battery M_b (9b). Furthermore, the torque at the wheel now depends on the mass, which is linear in m and can be approximated in a posynomial by using (9c).

$$m^M = \rho^M \bar{p}^{M,\text{out}} \quad (9a)$$

$$m \geq M_0 + M_d + M_a + M_b + m^M \quad (9b)$$

$$t_t^W \geq \delta_t m + \gamma_t \quad \forall t \in \mathcal{T} \quad (9c)$$

Additionally, we can easily extend the given model to account for recuperation. For this step, we have to model the fourth quadrant of the torque-speed domain with a second efficiency map model. This second model is comparable to the given model of the first quadrant, but differs slightly in the given parametrization. We can add the recuperation domain by using the absolute values of the given torque to map it to a new positive domain. In this domain, we use the newly defined efficiency map model and integrate it in the final model with a second weighted sum in constraint (6b). To account for the relation between the driving and recuperation, we add further positive weights, which weigh both sides against each other.

The shown GP-approach is also suitable for the already mentioned stochastic representation. In this, we can use multiple scenarios and weights to represent the given uncertain driving conditions. To ensure robust final solutions of the optimized system that fulfill all desired drive conditions in the underlying representative driving cycle or probability density function, we have to add further loads that lay on the convex hull of each cluster or at least at the highest required power demands. They are added as constraints but do not affect the objective.

Within this contribution, we presented a white-box reference-based model for the motor efficiency. Next to this approach further more detailed component models can be cast as a geometric program. For instance a more detailed motor mass estimation besides the density based approach would be possible. Furthermore, each component model representation which can be represented as a quantity of monomial or posynomial constraints can be used. This is often possible by adding further variables as shown in the motor model. If it is not possible, we can also fit a posynomial approximation, as for instance shown by [33].

9 Summary and Conclusion

We presented a mixed-integer geometric programming model for the early design stage of battery electric vehicles. We showed that the optimal design of a given gearbox and electric motor can be represented as a convex program, without specific requirements on the variables and constraints. This easily extendable basic model can therefore be used in numerous possibilities. The presented model was developed based on publicly available software and the usage of an of-the-shelf optimizer. Therefore, it is easily applicable in industry and academia. System model details next to the motor efficiency and transmission ratios can be added easily to the shown model, which makes it very suitable for early design proof-of-concepts and the comparison of optimal powertrain designs with different system layouts or components. Additionally, we showed an extension to explicitly consider a discrete transmission ratio selection and an according control strategy. Within the future, we will extend this model with an explicit consideration of recuperation and evaluate the shown method in more detail with more driving cycles, larger datasets and potentially other optimization methods. Furthermore, this optimization approach can also be transferred to other domains of designing technical systems. Therefore, we present an example for the design of a water supply system that is based on [34].

References

- [1] Björn Nykvist and Måns Nilsson. Rapidly falling costs of battery packs for electric vehicles. *Nature Climate Change*, 5(4):329, 2015.

- [2] Kate Palmer, James E Tate, Zia Wadud, and John Nellthorp. Total cost of ownership and market share for hybrid and electric vehicles in the uk, us and japan. *Applied Energy*, 209:108–119, 2018.
- [3] Wenbo Li, Ruyin Long, and Hong Chen. Consumers’ evaluation of national new energy vehicle policy in china: An analysis based on a four paradigm model. *Energy Policy*, 99:33–41, 2016.
- [4] Ona Egbue and Suzanna Long. Barriers to widespread adoption of electric vehicles: An analysis of consumer attitudes and perceptions. *Energy Policy*, 48:717–729, 2012.
- [5] Emilia Silvas, Theo Hofman, Nikolce Murgovski, Pascal Etman, and Maarten Steinbuch. Review of Optimization Strategies for System-Level Design in Hybrid Electric Vehicles. *IEEE Transactions on Vehicular Technology*, page 1, 2016.
- [6] Andreas Schönknecht, Adam Babik, and Viktor Rill. Electric powertrain system design of BEV and HEV applying a multi objective optimization methodology. *Transportation Research Procedia*, 14:3611–3620, 2016.
- [7] Senqi Tan, Jue Yang, Xinxin Zhao, Tingting Hai, and Wenming Zhang. Gear ratio optimization of a multi-speed transmission for electric dump truck operating on the structure route. *Energies*, 11(6):1324, 2018.
- [8] Paul D Walker, Salisa Abdul Rahman, Bo Zhu, and Nong Zhang. Modelling, simulations, and optimisation of electric vehicles for analysis of transmission ratio selection. *Advances in Mechanical Engineering*, 5:340435, 2013.
- [9] R. Duffin, E. Peterson, and C. Zener. *Geometric Programming – Theory and Application*. Wiley, New York, 1967.
- [10] Stephen Boyd, Seung-Jean Kim, Lieven Vandenbergh, and Arash Hassibi. A tutorial on geometric programming. *Optimization and Engineering*, 8(1):67, 2007.
- [11] Stephen Boyd and Lieven Vandenbergh. *Convex optimization*. Cambridge University Press, 2004.
- [12] Warren Hoburg and Pieter Abbeel. Geometric programming for aircraft design optimization. *AIAA Journal*, 52(11):2414–2426, 2014.
- [13] Michael J. Burton and Warren W. Hoburg. Solar-Electric and Gas Powered, Long-Endurance UAV Sizing via Geometric Programming. In *18th AIAA/ISSMO Multidisciplinary Analysis and Optimization Conference 2017*, Red Hook, NY, 2017? Curran Associates Inc.
- [14] Nikolce Murgovski, Lars Johannesson, Jonas Sjöberg, and Bo Egardt. Component sizing of a plug-in hybrid electric powertrain via convex optimization. *Mechatronics*, 22(1):106–120, 2012.
- [15] Nikolce Murgovski, Lars Mårdh Johannesson, and Jonas Sjöberg. Engine on/off control for dimensioning hybrid electric powertrains via convex optimization. *IEEE Transactions on Vehicular Technology*, 62(7):2949–2962, 2013.
- [16] Bo Egardt, Nikolce Murgovski, Mitra Pourabdollah, and Lars Johannesson Mardh. Electromobility studies based on convex optimization: Design and control issues regarding vehicle electrification. *IEEE Control Systems Magazine*, 34(2):32–49, 2014.
- [17] Xiaosong Hu, Yuan Zou, and Yalian Yang. Greener plug-in hybrid electric vehicles incorporating renewable energy and rapid system optimization. *Energy*, 111:971–980, 2016.
- [18] Dai-Duong Tran, Majid Vafaiepour, Mohamed El Baghdadi, Ricardo Barrero, Joeri van Mierlo, and Omar Hegazy. Thorough state-of-the-art analysis of electric and hybrid vehicle powertrains: Topologies and integrated energy management strategies. *Renewable and Sustainable Energy Reviews*, 119:109596, 2020.
- [19] Pierre Caillard, Frederic Gillon, Michel Hecquet, Sid-Ali Randi, and Noelle Janiaud. An optimization methodology to pre design an electric vehicle powertrain. In *2014 IEEE Vehicle Power and Propulsion Conference (VPPC)*, pages 1–6. IEEE, 2014.
- [20] Alexander Wasserburger, Christoph Hametner, and Nico Didcock. Risk-averse real driving emissions optimization considering stochastic influences. *Engineering Optimization*, 52(1):122–138, 2020.
- [21] Manfred Mitschke and Henning Wallentowitz. *Dynamik der Kraftfahrzeuge*, volume 5. Springer, 2014.
- [22] Monica Tutuianu, Alessandro Marotta, Heinz Steven, Eva Ericsson, Takahiro Haniu, Noriyuki Ichikawa, and Hajime Ishii. Development of a world-wide worldwide harmonized light duty driving test cycle (WLTC). *Draft Technical Report, DHC subgroup, GRPE-67-03*, 2013.
- [23] Patrick Christoph Vratny. *Conceptual Design Methods of Electric Power Architectures for Hybrid Energy Aircraft*. PhD thesis, Technische Universität München, 2019.
- [24] Amin Mahmoudi, Wen L Soong, Gianmario Pellegrino, and Eric Armando. Efficiency maps of electrical machines. In *2015 IEEE Energy Conversion Congress and Exposition (ECCE)*, pages 2791–2799. IEEE, 2015.

- [25] Jeongki An and Andreas Binder. Operation Strategy with Thermal Management of E-Machines in Pure Electric Driving Mode for Twin-Drive-Transmission (DE-REX). In *2017 IEEE Vehicle Power and Propulsion Conference (VPPC)*, Piscataway, NJ, 2017. IEEE.
- [26] Edward Burnell, Nicole B Damen, and Warren Hoburg. Gpkit: A human-centered approach to convex optimization in engineering design. In *Proceedings of the 2020 CHI Conference on Human Factors in Computing Systems*, pages 1–13, 2020.
- [27] François Margot. Symmetry in integer linear programming. In *50 Years of Integer Programming 1958-2008*, pages 647–686. Springer, 2010.
- [28] Ronald L Graham, Donald E Knuth, and Oren Patashnik. *Concrete mathematics: a foundation for computer science*, volume 1. Addison-Wesley, 1990.
- [29] Donald E Knuth. *Art of computer programming*, volume 1. Addison-Wesley, 3 edition, 1997.
- [30] J.F. Benders. Partitioning procedures for solving mixed-variables programming problems. *Numerische Mathematik*, 4(1):238–252, 1962.
- [31] Ragheb Rahmaniani, Teodor Gabriel Crainic, Michel Gendreau, and Walter Rei. The benders decomposition algorithm: A literature review. *European Journal of Operational Research*, 259(3):801–817, 2017.
- [32] Arved Esser, Martin Zeller, Stéphane Foulard, and Stephan Rinderknecht. Stochastic Synthesis of Representative and Multidimensional Driving Cycles. *SAE International Journal of Alternative Powertrains*, 7(3):263–272, 2018.
- [33] Warren Hoburg, Philippe Kirschen, and Pieter Abbeel. Fitting geometric programming models to data. *Optimization and Engineering*, 2014.
- [34] Philipp Leise, Lena C Altherr, and Peter F Pelz. Energy-efficient design of a water supply system for skyscrapers by mixed-integer nonlinear programming. In *Operations Research Proceedings 2017*, pages 475–481. Springer, 2018.

Appendix

Table A1: We present in the following all instances ordered by its identification number (ID) that were used for the comparison of the Benders (B), heuristic (H) and brute force (BF) approach to solve the developed Mixed-Integer Geometric Program. B and BF lead to a gap of 0. All primal solutions (P) are given in the logarithmic GP space. The number of used iterations is given by “#it”.

ID	BF/P	B/P	B+H/P	H/P	B/#it	B+H/#it	BF/#it	CYCLE
1	9.87	9.87	9.87	9.87	20	16	127	Artemis Motorway
2	9.78	9.78	9.78	9.78	27	33	127	Artemis Motorway
3	9.95	9.95	9.95	9.95	23	25	127	Artemis Motorway
4	9.72	9.72	9.72	9.72	16	22	127	Artemis Motorway
5	9.89	9.89	9.89	9.89	25	26	127	Artemis Motorway
6	9.79	9.79	9.79	9.79	31	36	127	Artemis Motorway
7	9.3	9.3	9.3	9.3	20	22	127	FTP75
8	8.6	8.6	8.6	8.6	31	32	127	FTP75
9	9.42	9.42	9.42	9.42	19	21	127	FTP75
10	9.44	9.44	9.44	9.44	29	25	127	FTP75
11	9.17	9.17	9.17	9.17	27	26	127	FTP75
12	8.92	8.92	8.92	8.92	30	32	127	FTP75
13	9.12	9.12	9.12	9.14	18	17	127	IMS Alltracks
14	9.24	9.24	9.24	9.24	26	24	127	IMS Alltracks
15	9.12	9.12	9.12	9.12	24	24	127	IMS Alltracks
16	9.44	9.44	9.44	9.44	19	22	127	IMS Alltracks
17	9.24	9.24	9.24	9.24	26	32	127	IMS Alltracks
18	8.39	8.39	8.39	8.39	36	33	127	NYCC
19	8.6	8.6	8.6	8.61	32	35	127	NYCC
20	8.78	8.78	8.78	8.78	27	29	127	NYCC
21	8.96	8.96	8.96	8.96	28	28	127	NYCC
22	8.63	8.63	8.63	8.63	35	36	127	NYCC
23	8.91	8.91	8.91	8.92	27	29	127	NYCC
24	9.26	9.26	9.26	9.27	21	16	127	WLTC
25	8.93	8.93	8.93	8.93	34	22	127	WLTC
26	9.45	9.45	9.45	9.45	17	22	127	WLTC
27	9.41	9.41	9.41	9.42	22	18	127	WLTC
28	9.39	9.39	9.39	9.39	27	27	127	WLTC
29	9.35	9.35	9.35	9.36	23	20	127	WLTC
30	9.87	9.87	9.87	9.87	60	62	511	Artemis Motorway
31	9.94	9.94	9.94	9.94	59	58	511	Artemis Motorway
32	10.02	10.02	10.02	10.02	86	84	511	Artemis Motorway
33	10.08	10.08	10.08	10.09	59	59	511	Artemis Motorway
34	9.97	9.97	9.97	9.97	41	47	511	Artemis Motorway
35	9.05	9.05	9.05	9.05	55	59	511	FTP75
36	9.03	9.03	9.03	9.03	39	41	511	FTP75
37	9.23	9.23	9.23	9.24	53	57	511	FTP75
38	9.13	9.13	9.13	9.13	37	39	511	FTP75
39	8.81	8.81	8.81	8.81	63	70	511	FTP75
40	9.34	9.34	9.34	9.34	45	50	511	FTP75
41	9.48	9.48	9.48	9.48	34	35	511	IMS Alltracks
42	9.02	9.02	9.02	9.02	50	51	511	IMS Alltracks
43	9.31	9.31	9.31	9.31	38	43	511	IMS Alltracks
44	9.4	9.4	9.4	9.41	34	33	511	IMS Alltracks
45	9.37	9.37	9.37	9.38	41	41	511	IMS Alltracks
46	8.35	8.35	8.35	8.35	86	94	511	NYCC
47	8.59	8.59	8.59	8.59	68	61	511	NYCC
48	8.86	8.86	8.86	8.86	85	83	511	NYCC
49	8.63	8.63	8.63	8.63	65	61	511	NYCC
50	8.93	8.93	8.93	8.93	54	53	511	NYCC
51	8.56	8.56	8.56	8.56	66	66	511	NYCC
52	9.27	9.27	9.27	9.27	56	61	511	WLTC
53	9.41	9.41	9.41	9.42	58	60	511	WLTC
54	9.55	9.55	9.55	9.56	47	44	511	WLTC
55	9.43	9.43	9.43	9.43	51	61	511	WLTC
56	9.51	9.51	9.51	9.51	44	61	511	WLTC
57	9.58	9.58	9.58	9.58	38	41	511	WLTC
58	9.86	9.86	9.86	9.86	102	105	2,047	Artemis Motorway
59	9.77	9.77	9.77	9.77	133	128	2,047	Artemis Motorway
60	9.96	9.96	9.96	9.96	108	113	2,047	Artemis Motorway
61	9.46	9.46	9.46	9.46	18	22	127	IMS Alltracks
62	9.75	9.75	9.75	9.75	58	57	511	Artemis Motorway
63	9.19	9.19	9.19	9.19	45	50	511	IMS Alltracks
64	9.93	9.93	9.93	9.93	130	130	2,047	Artemis Motorway
65	9.05	9.05	9.05	9.06	169	161	2,047	NYCC
66	9.67	9.67	9.67	9.67	8	8	31	Artemis Motorway
67	10.21	10.21	10.21	10.21	132	133	2,047	Artemis Motorway
68	10.08	10.08	10.08	10.08	126	130	2,047	Artemis Motorway
69	9.32	9.32	9.32	9.32	112	110	2,047	FTP75
70	8.9	8.9	8.9	8.9	112	127	2,047	FTP75
71	9.2	9.2	9.2	9.2	97	98	2,047	FTP75
72	9.27	9.27	9.27	9.27	133	146	2,047	FTP75

73	9.37	9.37	9.37	9.37	119	120	2,047	FTP75
74	9.29	9.29	9.29	9.29	88	81	2,047	FTP75
75	9.26	9.26	9.26	9.26	85	88	2,047	IMS Alltracks
76	9.3	9.3	9.3	9.31	83	77	2,047	IMS Alltracks
77	9.54	9.54	9.54	9.54	86	91	2,047	IMS Alltracks
78	9.4	9.4	9.4	9.4	67	60	2,047	IMS Alltracks
79	9.7	9.7	9.7	9.7	69	67	2,047	IMS Alltracks
80	9.59	9.59	9.59	9.59	95	95	2,047	IMS Alltracks
81	8.83	8.83	8.83	8.84	162	170	2,047	NYCC
82	8.91	8.91	8.91	8.91	147	142	2,047	NYCC
83	9.03	9.03	9.03	9.03	165	148	2,047	NYCC
84	8.99	8.99	8.99	8.99	140	138	2,047	NYCC
85	9.06	9.06	9.06	9.06	176	164	2,047	NYCC
86	9.46	9.46	9.46	9.46	95	98	2,047	WLTC
87	9.58	9.58	9.58	9.58	108	108	2,047	WLTC
88	9.66	9.66	9.66	9.66	106	104	2,047	WLTC
89	9.51	9.51	9.51	9.51	97	99	2,047	WLTC
90	9.63	9.63	9.63	9.63	111	115	2,047	WLTC
91	9.72	9.72	9.72	9.72	157	152	2,047	WLTC
92	9.58	9.58	9.58	9.59	8	8	31	Artemis Motorway
93	9.1	9.1	9.1	9.1	12	14	31	Artemis Motorway
94	8.98	8.98	8.98	8.99	15	8	31	Artemis Motorway
95	9.06	9.06	9.06	9.06	12	11	31	Artemis Motorway
96	9.48	9.48	9.48	9.48	8	7	31	Artemis Motorway
97	8.09	8.09	8.09	8.09	16	17	31	FTP75
98	8.98	8.98	8.98	8.98	10	11	31	FTP75
99	9.16	9.16	9.16	9.19	9	9	31	FTP75
100	8.84	8.84	8.84	8.84	9	8	31	FTP75
101	8.82	8.82	8.82	8.84	9	7	31	FTP75
102	9.04	9.04	9.04	9.04	8	9	31	FTP75
103	8.65	8.65	8.65	8.65	15	13	31	IMS Alltracks
104	9.24	9.24	9.24	9.24	10	10	31	IMS Alltracks
105	9.17	9.17	9.17	9.17	8	9	31	IMS Alltracks
106	8.93	8.93	8.93	8.93	12	9	31	IMS Alltracks
107	8.77	8.77	8.77	8.77	13	13	31	IMS Alltracks
108	9.13	9.13	9.13	9.13	10	14	31	IMS Alltracks
109	8.56	8.56	8.56	8.56	8	8	31	NYCC
110	8.54	8.54	8.54	8.54	9	10	31	NYCC
111	8.09	8.09	8.09	8.09	9	10	31	NYCC
112	7.89	7.89	7.89	7.89	12	13	31	NYCC
113	8.54	8.54	8.54	8.54	9	13	31	NYCC
114	8.75	8.75	8.75	8.75	8	8	31	NYCC
115	9.08	9.08	9.08	9.08	8	9	31	WLTC
116	8.88	8.88	8.88	8.89	7	7	31	WLTC
117	9.1	9.1	9.1	9.1	10	9	31	WLTC
118	9.21	9.21	9.21	9.21	9	7	31	WLTC
119	8.64	8.64	8.64	8.64	12	10	31	WLTC
120	8.64	8.64	8.64	8.64	10	11	31	WLTC